ACS Combinatorial Science
Research Article
pubs.acs.org/acscombsci

Full Range Dielectric Characteristics of Calcium Copper Titanate Thin Films Prepared by Continuous Composition-Spread Sputtering

Hyo Min Kang,[†,‡] Seung-Hyub Baek,[†,§] Jong Han Song,[#] Yong Soo Cho,[*,‡] and Ji-Won Choi[*,†,§]

[†]Electronic Materials Research Center, Korea Institute of Science and Technology, Seoul, 136-791, Republic of Korea
[‡]Departments of Materials Science and Engineering, Yonsei University, Seoul, 120-749, Republic of Korea
[§]Department of Nanomaterials Science and Technology, University of Science and Technology, Daejeon, 305-333, Republic of Korea
[#]Advanced Analysis Center, Korea Institute of Science and Technology, Seoul, 136-791, Republic of Korea

ABSTRACT: Perovskite $CaCu_3Ti_4O_{12}$ has drawn a great deal of attention for various electronic applications due to its giant dielectric property as well as a strong stability in a wide range of temperature. In this paper, we use an off-axis continuous composition-spread (CCS) sputtering method to investigate the full range dielectric characteristics of calcium copper titanate thin films. The film compositions are continuously distributed by deposition from two targets of $CaTiO_3$ and $CuTiO_3$. A slightly Ca-deficient, Cu- and Ti-rich film, which has a 0.9:3.2:4.3 ratio for Ca:Cu:Ti, demonstrated the best performance by showing a dielectric constant of 781 at 100 kHz. On the other hand, all other films far away from the $CaCu_3Ti_4O_{12}$ composition showed suppressed dielectric properties. Analyses by X-ray photon spectroscopy, micro-Raman microscopy, transmission electron microscopy, and Rutherford backscattering spectroscopy reveal that there are three possible origins for such superior performance at off stoichiometric thin films: (1) bulk doping by excessive Cu and Ti ions, (2) chemically modified grain boundary, and (3) the lowered electrode−sample interface resistance. Our result will provide a new insight into engineering the dielectric properties using off-stoichiometric synthesis.

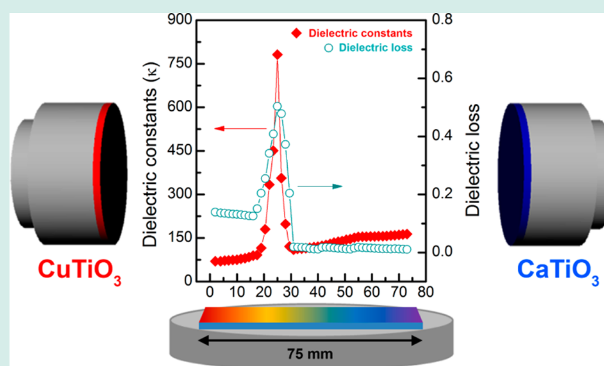

KEYWORDS: *$CaCu_3Ti_4O_{12}$, continuous composition spread, sputtering, dielectric properties, thin films*

■ INTRODUCTION

In last decades, the electronic industry has pursued competitive materials with exceptionally outstanding properties for improving performance and miniaturization of the dimensions of electronic components. As a critical part of the electronic components, dielectric materials have been extensively studied, with efforts to optimizing the design and structure of components. Dielectric materials, particularly those having higher dielectric constant k and less dependence on temperature within the operational ranges of frequency and temperature, have been regarded as promising for very recent electronic applications demanding the minimization of the occupancy volume of components. Although conventional high k ferroelectric materials, including $BaTiO_3$, $MgSnO_3$, $SrTiO_3$, and $Pb(Mg_{1/3}Nb_{2/3})O_3$, have been actively utilized for commercial components, there has always been demand for higher k and better stability against degradation by high temperature.[1−3] As an alternative candidate, another perovskite calcium copper titanate having stoichiometric $CaCu_3Ti_4O_{12}$ composition has emerged, mainly due to its unusually high dielectric performance.[4,5] Bulk $CaCu_3Ti_4O_{12}$ materials have giant permittivity of $\sim 10^4 \sim 10^5$ at kHz and the least dependence of k over the broad temperature range from 100 to 400 K.[6,7]

Although many groups have proposed dielectric models to explain the origin of the giant dielectric constant of $CaCu_3Ti_4O_{12}$, it has still not been thoroughly understood. At present, many papers based on the impedance analysis reported that the dielectric phenomenon of $CaCu_3Ti_4O_{12}$ is mostly affected by extrinsic factors such as the depletion layer at the grain boundary or between the sample surface and the electrodes. This aspect may be most viable in explaining the origin of the extraordinary dielectric behavior as the insulating barriers between semiconducting regions.[8−10] Low resistance of grain and high resistance of depletion layer are responsible for the origin of the dielectric constant. Secondary phases occupying the grain boundary region or grain junctions are reported to act as a source of either the highly insulating nature of the grain boundary or the inhibited motion of the grain boundary.[11−15]

There have been relatively limited studies on the characteristics of $CaCu_3Ti_4O_{12}$ thin films and their correlative dependency of compositional fluctuations on dielectric performance. Among many conventional thin film processes, the continuous

Received: April 9, 2014
Revised: July 8, 2014
Published: July 16, 2014

 © 2014 American Chemical Society

composition spread (CCS) approach that utilizes cosputter depositions between designated targets may be very useful in understanding the compositional sensitivity of dielectric properties and defining the optimal stoichiometry in terms of performance. The CCS approach allows the multicomponent or multiphase system to be fully analyzed in the full range of composition between end-members in a single trial of deposition.[16−19] It often leads to unusual stoichiometry composition with unexpected characteristics.

In this work, CCS sputtering between the targets of $CaTiO_3$ and $CuTiO_3$ is conducted to define the detailed compositional dependence of the dielectric properties around the known $CaCu_3Ti_4O_{12}$ compound. An optimal composition having a certain Ca:Cu:Ti ratio other than a stoichiometric one may be suggested with the enhanced dielectric properties. The valence state of the cations and complex impedance analysis are carried out to support the observed dielectric properties.

RESULTS AND DISCUSSION

Figure 1b shows the thickness profiles of the CCS thin films along the sample length between the target locations of $CaTiO_3$ and $CuTiO_3$, which were obtained by the direct observation from cross-sectional SEM images. The thickness was plotted as a function of the distance from the $CuTiO_3$ target toward the $CaTiO_3$ target. The points from P1 to P7 were marked as the dashed straight lines. To understand the thickness profile, thin films only from each target were separately deposited, and their thickness was monitored. The thickness distributions of films deposited from each $CaTiO_3$ or $CuTiO_3$ target were also plotted as shown in Figure 1b. The resultant thickness variation of the CCS films follows the deposition rates of films from each

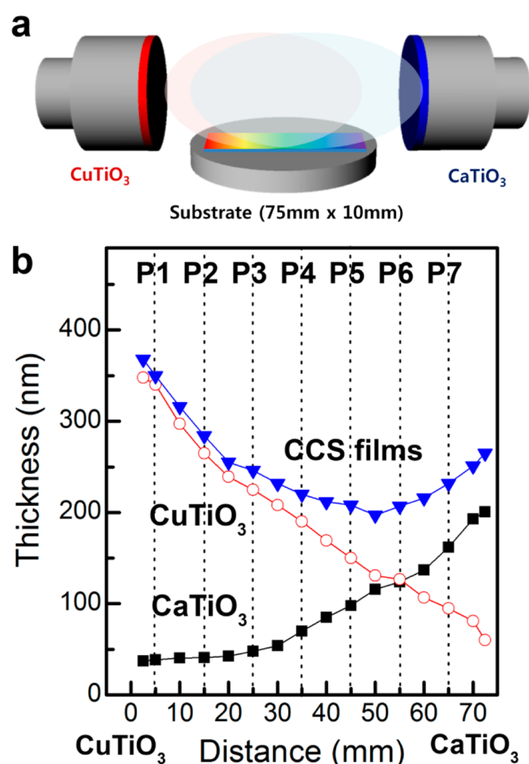

Figure 1. (a) Schematic diagram of the off-axis RF sputtering CCS system and (b) thickness profiles of $CaTiO_3$, $CuTiO_3$, and CCS thin films at 70 W.

target over the sample length. For instance, the varying tendency of CCS film thickness matches well to the summation of thickness of films from each $CaTiO_3$ or $CuTiO_3$ target at each point.[16,19] The total thickness of the CCS films ranged from ∼200 to 350 nm. Differences in sputter yields and resultant deposition rates are attributed to determine the thickness dependence of the CCS films over the given length.

Figure 2 shows the XRD patterns of the CCS thin films at each point. The $CaCu_3Ti_4O_{12}$ crystalline phase was observed

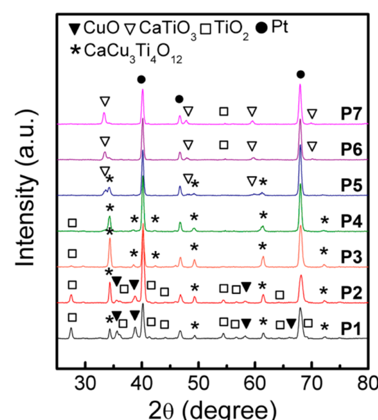

Figure 2. X-ray diffraction patterns of the CCS thin films at each designated point.

over all the compositional range except P7, but the $CaCu_3Ti_4O_{12}$ phase was dominant only at points of P2 to P5. As expected, the $CaTiO_3$ phase was dominantly found at P6 and P7, since the points are close to the $CaTiO_3$ target. Interestingly, however, the location at P1 did not show the $CuTiO_3$ phase but the phases of CuO and TiO_2 were distinctly observed. The location at P3 corresponds to an almost-pure $CaCu_3Ti_4O_{12}$ phase. All other locations seem to contain the secondary phase such as $CaTiO_3$ or CuO, depending on the distance from each target.

It is reasonably conclusive that deficient or an excess of Ca, Cu, and Ti elements away from the stoichiometric $CaCu_3Ti_4O_{12}$ compound creates the distribution of different phases over the sample length.

For further structural analysis, micro-Raman spectra measurement with a beam size of 1 μm was performed for the additional points only around P3 as designated as A, B, C(P3), D($CaCu_3Ti_4O_{12}$), and E in the schematic of Figure 3a. The distance between additional neighboring points was ∼1.5 mm. As shown in Figure 3b, the scattering peaks of crystalline $CaCu_3Ti_4O_{12}$ modes were clearly observed, as they correspond to $F_g(1)$ at 292 cm^{-1}, $A_g(1)$ at 445 cm^{-1}, $A_g(2)$ at 511 cm^{-1}, and $F_g(3)$ at 576 cm^{-1} in all the samples.[20,21] The scattering modes of $F_g(1)$, $A_g(1)$, and $A_g(2)$ are associated with TiO_6 rotation-like vibrations. The $F_g(3)$ mode stands for O−Ti−O antistretching vibrations in $CaCu_3Ti_4O_{12}$. For the points A and B that are closer to the $CuTiO_3$ target, however, two additional variation peaks were observed with the gradual reduction in the intensity of the $A_g(1)$, $A_g(2)$ and $F_g(3)$ peaks. The two additional peaks appeared as A_g at 297 cm^{-1} and B_g at 627 cm^{-1}, which are associated with the CuO phase.[22]

The intensity decrease of the $A_g(1)$, $A_g(2)$, and $F_g(3)$ modes is related to the creation of Cu−O bonds with increasing Cu content beyond the $CaCu_3Ti_4O_{12}$ stoichiometry. The Cu−O bonds may impede the rotations of TiO_6 octahedrons in

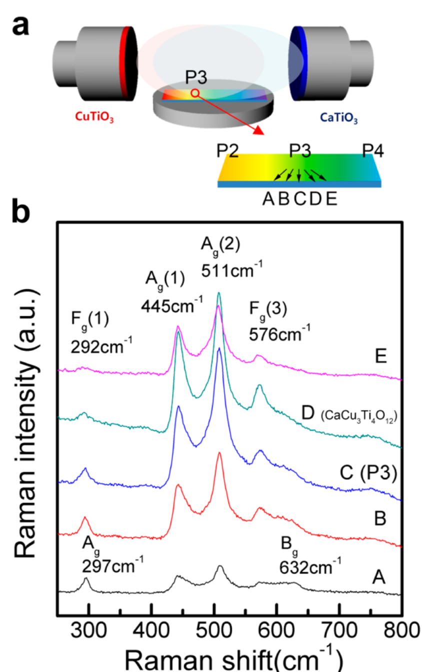

Figure 3. (a) Schematic of detailed points around P3 for the Raman analysis, and (b) micro-Raman spectra of the CCS thin films at the A, B, C, D, and E points.

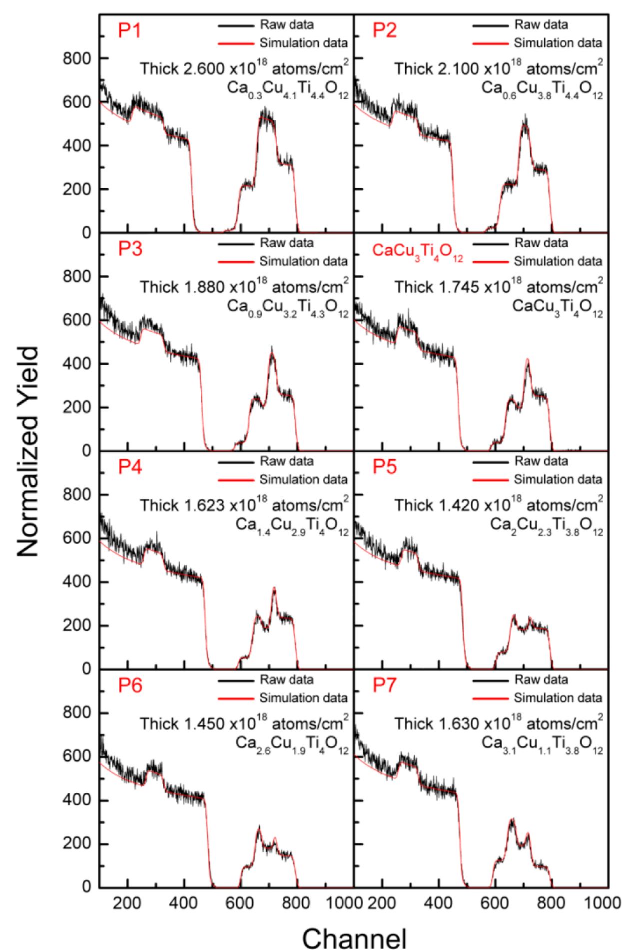

Figure 4. Two MeV $^{4}He^{2+}$ backscattering spectra obtained at each designated point of the CCS films.

$CaCu_3Ti_4O_{12}$, thus resulting in the reduction in the rotation mode intensity.[23]

In order to evaluate the overall changes in elemental ratios across the sample, 2 MeV $4He^{+2}$ backscattering spectroscopy (BS) measurements were carried out. The backscattering spectra were simulated by a RUMP code to obtain the concentration (atomic %) of each element for the P1−P7 points. The backscattering spectra and obtained concentration for P1−P7 are shown in Figure 4. The varying tendency of the relative atomic percentage with each point defined from the distance between the targets tends to match well with the phase evolution observed from the XRD patterns of Figure 2. The atomic Ca:Cu:Ti ratio of 0.9:3.2:4.3 observed at the P3 location turned out to be the most close to the $CaCu_3Ti_4O_{12}$ ratio of 1:3:4, and the $CaCu_3Ti_4O_{12}$ region also confirmed at around P3 an approach of 1.5 mm to the $CaTiO_3$ target. As anticipated, the relative content of Ca was found to increase gradually as the film location is heading toward the $CaTiO_3$ target. The atomic percentage of Cu has the same increasing tendency as the film approaches the $CuTiO_3$ target. Note that the atomic percentages at each point reflect the multiphases observed in the XRD patterns. Therefore, the ratios do not represent nonstoichiometric compounds.

XPS analysis was performed to investigate the oxidation states of constituent anions of the CCS films at P3 as shown in Figure 5. For comparison, the curves for $CaCu_3Ti_4O_{12}$ thin films are included. Figure 5a represents clearly the valence states of Cu ions as Cu^{3+}, Cu^{2+}, and Cu^{+} peaks are observed in the binding energy range of 930 to 938 eV. The Cu $2p_{3/2}$ spectrum came from the superposition of the spectra of Cu^{+}, Cu^{2+}, and Cu^{3+} as reported elsewhere.[24,25]

The locations of each ion in the P3 films are very similar to those obtained for the $CaCu_3Ti_4O_{12}$ films. On the other hand, the spectra of Figure 5b suggest the valence state of Ti ions at the binding energies of 456−462 eV. Distinct peaks of Ti^{4+} and Ti^{3+} ions, respectively, at 458.15 and 458.7 eV, in the P3 films were observed, as their peak locations are very close to those for the $CaCu_3Ti_4O_{12}$ films.[24,26] The Ti $2p_{3/2}$ peak of the P3 films corresponds to the superposition of the spectra of Ti^{3+} and Ti^{4+}.

From the calculation of each peak's area by the data fitting analysis, the area ratio of Cu^{+}:Cu^{2+}:Cu^{3+} was 0.22:1.00:0.15 for the P3 films and 0.174:1.00:0.18 for the $CaCu_3Ti_4O_{12}$ films, respectively. It indicates that Cu^{+} ions are more dominant in the P3 films compared to the $CaCu_3Ti_4O_{12}$ films. Similarly, the calculated area ratio of Ti^{3+}:Ti^{4+} was increased from 0.68:1.00 to 0.98:1.00 at P3 thin films compared to $CaCu_3Ti_4O_{12}$ films. The calculation of individual peak area suggests that the Ti^{3+} valence state becomes serious in the P3 films. Accordingly, the Cu^{+}/Cu^{2+} and Ti^{3+}/Ti^{4+} ratios are changed increasingly in the P3 films. This observation is believed to be associated with defect formations such as oxygen vacancies, which can induce easier dipole displacements in films.[24,27]

Figure 6a shows the variations in dielectric constant and loss of the CCS films measured on 200 μm × 200 μm capacitors at 100 kHz as a function of the distance from the $CuTiO_3$ target. The dielectric properties of the CCS films were dependent largely on the distance, as highlighted with prominent peaks at P3 in the plots of dielectric constant and loss. The peak dielectric constant value was around 781 at P3. As the distance increases from P3 to P7, the dielectric constant tends to increase, gradually reaching ∼150 at P7. The variation in dielectric properties is understood to be directly related to the

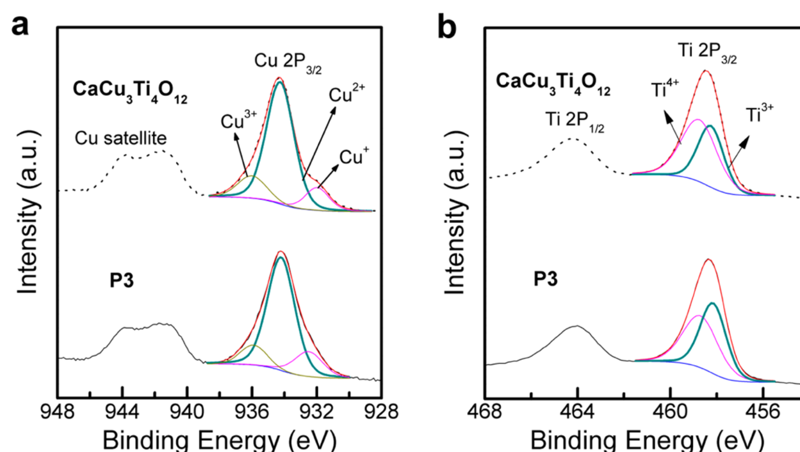

Figure 5. XPS spectra of the P3 films: (a) Cu 2p region and (b) Ti 2p region. For comparison, the spectra of stoichiometric $CaCu_3Ti_4O_{12}$ films are included.

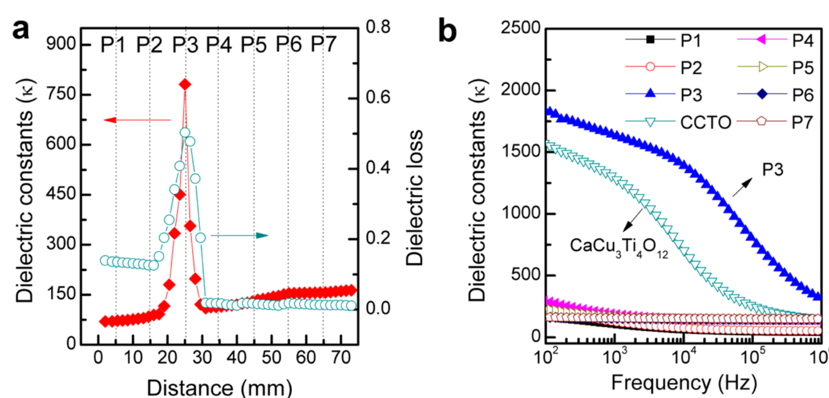

Figure 6. (a) Variations in dielectric constant and loss of the CCS films at 100 kHz as a function of each film location. (b) Frequency dependence of dielectric constant in each film location at room temperature.

phase evolutions observed in Figure 2. Compositions far away from the $CaCu_3Ti_4O_{12}$ stoichiometry (otherwise, less content of the $CaCu_3Ti_4O_{12}$ phase) in the CCS films are unlikely to produce high relative permittivity values. The frequency dependence of the dielectric constants was performed from 100 Hz to 1 MHz, as shown in Figure 6b. Each position shows that dielectric tendency varies with compositions difference. The high dielectric constants of P3 and $CaCu_3Ti_4O_{12}$ decreased slowly under 10 kHz, while the dielectric constant decreased sharply when frequency was passed over 10 kHz. The P3 films show higher dielectric constants (~1700) than $CaCu_3Ti_4O_{12}$ films (1350) at the frequency of 1 kHz. The dielectric constant of the $CaCu_3Ti_4O_{12}$ film is comparable to the previously reported values elsewhere.[28−30] However, points other than P3 and $CaCu_3Ti_4O_{12}$ show almost invariable dielectric constants along the frequency. The relaxation behaviors of dielectric constants at P3 and $CaCu_3Ti_4O_{12}$ are Debye-like and are consistent with the previous reports.[8−11,30] All other points except for the P3 and $CaCu_3Ti_4O_{12}$ points appear to be constant dielectric constants along the frequency, suggesting that the secondary phases other than the $CaCu_3Ti_4O_{12}$ phase act more critically in the dielectric constants. This shows that the contribution by grain boundary is not expected at these points.

Figure 7 shows high-resolution TEM image and EDS line profile results of the grain boundary region in the (a) P3 and (b) $CaCu_3Ti_4O_{12}$ films. The grain size of 80 nm for P3

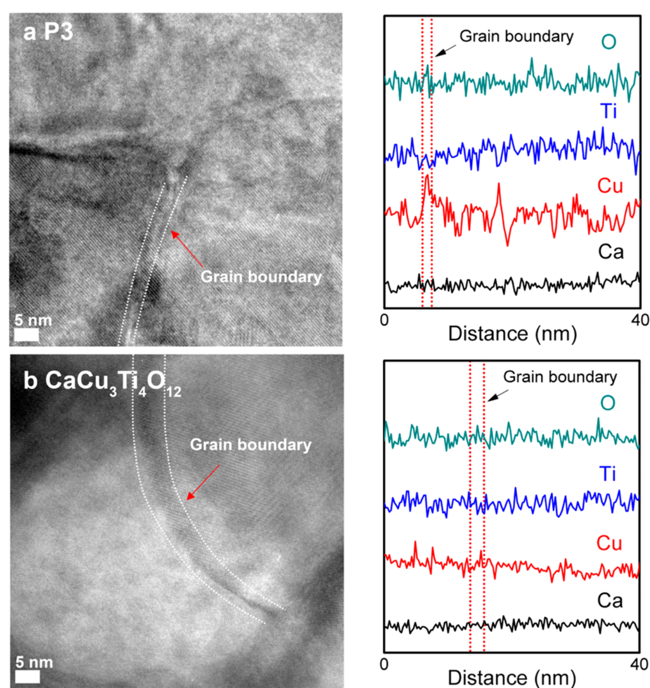

Figure 7. High-resolution TEM image and EDS line profile results of grain boundary region in the (a) P3 and (b) $CaCu_3Ti_4O_{12}$ films.

dx.doi.org/10.1021/co500057u | ACS Comb. Sci. 2014, 16, 478−484

confirms that it has an increased grain size compared to that for $CaCu_3Ti_4O_{12}$ of 70 nm.

Also, the thickness of the grain boundary in P3 films seems to be reduced from 2.2 to 1.5 nm by Cu and Ti substitution. However, precise comparison of the grain boundary thickness in P3 and $CaCu_3Ti_4O_{12}$ was difficult to make clear. Based on the observations, P3 has bigger grains and a reduced grain boundary compared to $CaCu_3Ti_4O_{12}$, and the relationship between grain/grain boundary ratio and dielectric constant is already described in many reports.[12,27,31,32] The EDS line profile results of P3 and $CaCu_3Ti_4O_{12}$ reveal increasing Cu content at the grain boundaries in P3; however, no segregation of Ca, Cu, Ti, and O was found along the grain boundaries in $CaCu_3Ti_4O_{12}$. Excessive Cu was segregated along the grain boundary, resulting in the chemically and structurally modified grain boundary as well as the grain growth rate.[12,13,32]

Figure 8a shows the complex impedance curves of the CCS thin films at each point. For comparison, the cole−cole plot of the $CaCu_3Ti_4O_{12}$ film is also shown. Generally, the maximum point of the imaginary part (Z'') of the complex impedance follows the given formula

$$R_{gb}C_{gb} = 1/(2\pi f) \quad (1)$$

where R is the resistance, C is the capacitance, and f is the oscillating frequency. The grain, grain boundary, and electrode−sample interface contributions are separately analyzed only when a clear semicircle is obtained. Approaching CCS sputtering made limited compositional homogeneous regions along the locations, and it caused an overlapped semicircle of all the components at P3 and $CaCu_3Ti_4O_{12}$.

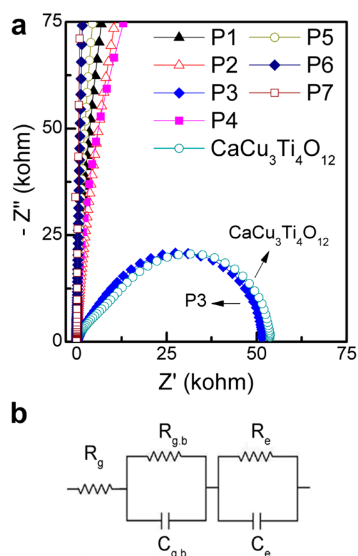

Figure 8. (a) Complex impedance curves of the CCS thin films at each point and (b) schematic of equivalent circuit.

From the equivalent circuits for P3 and $CaCu_3Ti_4O_{12}$ in Figure 8b, one R_g element corresponded to the semiconducting grains, which have resistance values of 97 Ω and 127 Ω for the P3 and $CaCu_3Ti_4O_{12}$ films, respectively. The grain boundary contributions were found in P3 films as $R_{gb} \sim 6.5$ kΩ and $C_{gb} \sim 0.27$ nF. Particularly, $R_{gb} \sim 9.3$ kΩ of the $CaCu_3Ti_4O_{12}$ film is larger than the R_{gb} value of the P3 film. Also, the RC component of the electrode−sample interface of $R_{ele} \sim 41$ kΩ and $C_{ele} \sim 1.91$ nF for P3 and $R_{ele} \sim 41.5$ kΩ and $C_{ele} \sim 1.70$ nF for $CaCu_3Ti_4O_{12}$ were confirmed, respectively. As a result, electrical inhomogeneities with the grain, grain boundary, and electrode−sample interface contribute to the realization of a high dielectric constant. Increasing of metallic Cu contents at the grain boundary reduces the R_{gb} in the P3 film, as shown in EDS results of Figure 7. And smaller R_{gb} and R_{ele} in the P3 film is likely to contribute to the enhanced dielectric properties as elsewhere.[8,11,31,32] Increasing of secondary phases around the $CaCu_3Ti_4O_{12}$ phase acts more critically at other points without P3 and $CaCu_3Ti_4O_{12}$. Thus, all other points except for P3 and $CaCu_3Ti_4O_{12}$ demonstrate no cole−cole plots in the impedance results. No influence of depletion layer at the grain boundary or electrode−sample interface shows invariable dielectric constants as shown in Figure 6b.

■ CONCLUSION

Calcium copper titanate films having continuous composition-spread between $CaTiO_3$ and $CuTiO_3$ are investigated to understand the influence of composition change on their dielectric properties. A slightly off-stoichiometric film rather than stoichiometric $CaCu_3Ti_4O_{12}$ turned out to be the optimal composition by generating the highest dielectric constant of 781 at 100 kHz. We proposed three possible origins: (1) bulk doping effect by nonstoichiometric anions, (2) chemically modified grain boundary, and (3) lower electrode−sample interface resistance. Beyond dielectric materials, our result will open a new avenue to engineer the physical properties of various functional materials using an off-stoichiometric synthesis method.

■ EXPERIMENTAL PROCEDURES

The full range of calcium copper titanate composition was investigated by the off-axis CCS sputtering between the targets of $CaTiO_3$ (2 in., purity 99.99%, Toshima Manufacturing Co., Ltd.) and $CuTiO_3$ (2 in., purity 99.99%, LTS Chemical Inc.). As seen in the schematic of the sputtering configuration in Figure 1a, the off-axis CCS sputter system has two independent radio frequency (RF) magnetron sputtering guns that are positioned at each end and perpendicularly to the substrate. Thin films were grown on a Pt(111)/Ti/SiO_2/Si substrate (75 mm × 10 mm) at 500 °C for 3 h under argon and oxygen mixed pressure (8:2) of 20 mTorr. An identical RF power of 70 W was applied to each target of $CaTiO_3$ and $CuTiO_3$. After the CCS deposition, the samples were annealed at 750 °C in O_2 atmosphere for 10 min by rapid thermal annealing (RTA). Then the Pt top electrode was deposited in a multisquare (200 × 200 μm^2 each) pattern onto the films by DC sputtering to form metal−insulator−metal (MIM) capacitor structures. As illustrated in Figure 1a, a total of seven different points, P1 to P7, allocated from each end with an equal distance (∼10 mm) between the neighboring points, are selected for this compositional dependency study.

The cross-section and thickness of the thin films were examined with an environmental scanning electron microscope (ESEM; XL-30 FEG, Ph ilips). The structural properties and composition of the thin films were characterized by transmission electron microscopy (TEM; Titan TM 80-300, FEI), X-ray diffraction (XRD; X'pert Pro, PANalytical) analysis, micro-Raman spectroscopy (Renishaw In-Via Raman Microscope, Renishaw), and Rutherford backscattering spectroscopy (NEC, 6SDH2). The chemical properties of the film surface were analyzed by X-ray photoelectron spectroscopy (XPS, PHI

X-tool, ULVAC-PHI, Inc.) Dielectric properties and their frequency dependence at each point of the films were measured in the frequency range of 40 Hz to 1 MHz at room temperature by an impedance analyzer (4294A, Agilent).

■ AUTHOR INFORMATION

Corresponding Authors

*Tel: +82-2-958-5556, Fax: +82-2-958-6720, jwchoi@kist.re.kr.
*Tel: +82-2-2123-5848, Fax: +82-2-312-5375, ycho@yonsei.ac.kr.

Author Contributions

H.M.K. performed film deposition and dielectric measurements. J.H.S. carried out RBS measurement and analysis. J.-W.C. and Y.S.C. supervised the experiments and contributed to manuscript preparation. H.M.K., S.-H.B., Y.S.C., and J.-W.C. analyzed the data and wrote the manuscript. J.-W.C. conceived the idea and initiated and directed the research. All authors discussed the progress of research and reviewed the manuscript. The manuscript was written through contributions of all authors. All authors have given approval to the final version of the manuscript.

Notes

The authors declare no competing financial interest.

■ ACKNOWLEDGMENTS

This study was supported by the Core Technology of Materials Research and Development Program (No. 10041232) funded by the Ministry of Trade, Industry & Energy, and also partially by the National Research Foundation of Korea (NRF) (Grant No. 2011-0020285).

■ REFERENCES

(1) Chung, S. Y.; Kim, I. D.; Kang, S. J. L. Strong nonlinear current−voltage behaviour in perovskite-derivative calcium copper titanate. *Nat. Mater.* **2004**, *3*, 774−778.
(2) Ramírez, M. A.; Bueno, P. R.; Tararam, R. A.; Cavalheiro, A.; Longo, E.; Varela, J. A. Evaluation of the effect of the stoichiometric ratio of Ca/Cu on the electrical and microstructural properties of the $CaCu_3Ti_4O_{12}$ polycrystalline system. *J. Phys. D: Appl. Phys.* **2009**, *42*, 185503.
(3) Kwon, S.; Cann, D. P. Influence of the processing rates and sintering temperatures on the dielectric properties of $CaCu_3Ti_4O_{12}$ ceramics. *J. Electroceram.* **2010**, *24*, 231−236.
(4) Subramanian, M. A.; Li, D.; Duan, N.; Reisner, B. A.; Sleight, A. W. High Dielectric Constant in $ACu_3Ti_4O_{12}$ and $ACu_3Ti_3FeO_{12}$ Phases. *J. Solid State Chem.* **2000**, *151*, 323−325.
(5) Homes, C. C.; Vogt, T. S.; Shapiro, M.; Wakimoto, S.; Ramirez, A. P. Optical Response of High-Dielectric-Constant Perovskite-Related Oxide. *Science* **2001**, *293*, 673−676.
(6) Foschini, C. R.; Tararam, R.; Simões, A. Z.; Cilense, M.; Longo, E.; Varel, J. A. $CaCu_3Ti_4O_{12}$ thin films with non-linear resistivity deposited by RF-sputtering. *J. Alloys Compd.* **2013**, *574*, 604−608.
(7) Li, J.; Subramanian, M. A.; Rosenfeld, H. D.; Jones, C. Y.; Toby, B. H.; Sleight, A. W. Clues to the Giant Dielectric Constant of $CaCu_3Ti_4O_{12}$ in the Defect Structure of "$SrCu_3Ti_4O_{12}$". *Chem. Mater.* **2004**, *16*, 5223−5225.
(8) Adams, T. B.; Sinclair, D. C.; West, A. R. Giant Barrier Layer Capacitance Effect in $CACu_3Ti_4O_{12}$ Ceramics. *Adv. Mater.* **2002**, *14*, 1321−1323.
(9) Sinclair, D. C.; Adams, T. B.; Morrison, F. D.; West, A. R. $CaCu_3Ti_4O_{12}$: One-step internal barrier layer capacitor. *Appl. Phys. Lett.* **2002**, *80*, 2153−2155.
(10) Lin, Y. H.; Li, M.; Nan, C. W.; Li, J. Grain and grain boundary effects in high-permittivity dielectric NiO-based ceramics. *Appl. Phys. Lett.* **2006**, *89*, 132907.
(11) Schmidt, R.; Stennett, M. C.; Hyatt, N. C.; Pokorny, J.; Prado-Gonjal, J.; Li, M.; Sinclair, D. C. Effects of sintering temperature on the internal barrier layer capacitor (IBLC) structure in $CaCu_3Ti_4O_{12}$ (CCTO) ceramics. *J. Eur. Ceram. Soc.* **2012**, *32*, 3313−3323.
(12) Mei, L. T.; Hsiang, H. I.; Fang, T. T. Effect of Copper-Rich Secondary Phase at the Grain Boundaries on the Varistor Properties of $CaCu_3Ti_4O_{12}$ Ceramics. *J. Am. Ceram. Soc.* **2008**, *91*, 3735−3737.
(13) Fang, T. T.; Mei, L. T.; Ho, H. F. Effects of Cu stoichiometry on the microstructures, barrier-layer structures, electrical conduction, dielectric responses, and stability of $CaCu_3Ti_4O_{12}$. *Acta Mater.* **2006**, *54*, 2867−2875.
(14) Marchin, L.; Guillemet-Fritsch, S.; Durand, B. Grain Growth-Controlled Giant Permittivity in Soft Chemistry $CaCu_3Ti_4O_{12}$ Ceramics. *J. Am. Ceram. Soc.* **2008**, *91*, 485−489.
(15) Zhang, L. Electrode and grain-boundary effects on the conductivity of $CaCu_3Ti_4O_{12}$. *Appl. Phys. Lett.* **2005**, *87*, 022907.
(16) van Dover, R. B.; Schneemeyer, L. F.; Fleming, R. M. Discovery of a useful thin-film dielectric using a composition-spread approach. *Nature* **1998**, *392*, 162−164.
(17) Takeuchi, I.; Famodu, O. O.; Read, J. C.; Aronova, M. A.; Chan, K.-S.; Craciunescu, C.; Lofland, S. E.; Wuttig, M.; Wellstood, F. C.; Knauss, L.; Orozco, A. Identification of novel compositions of ferromagnetic shape-memory alloys using composition spreads. *Nat. Mater.* **2003**, *2*, 180−184.
(18) van Dover, R. B.; Schneemeyer, L. F. The Codeposited Composition Spread Approach to High-Throughput Discovery/Exploration of Inorganic Materials. *Macromol. Rapid Commun.* **2004**, *25*, 150−157.
(19) Jung, K.; Choi, W. K.; Yoon, S. J.; Kim, H. J.; Choi, J. W. Electrical and optical properties of Ga doped zinc oxide thin films deposited at room temperature by continuous composition spread. *Appl. Surf. Sci.* **2010**, *256*, 6219−6223.
(20) Kolev, N.; Bontchev, R. P.; Jacobson, A. J.; Popov, V. N.; Hadjiev, V. G.; Litvinchuk, A. P.; Iliev, M. N. Raman spectroscopy of $CaCu_3Ti_4O_{12}$. *Phys. Rev. B* **2002**, *66*, 132102.
(21) Valim, D.; Souza Filho, A. G.; Freire, P. T. C.; Fagan, S. B.; Ayala, A. P.; Mendes Filho, J.; Almeida, A. F. L.; Fechine, P. B. A.; Sombra, A. S. B.; Staun Olsen, J.; Gerward, L. Raman scattering and x-ray diffraction studies of polycrystalline $CaCu_3Ti_4O_{12}$ under high-pressure. *Phys. Rev. B* **2004**, *70*, 132103.
(22) Litvinchuk, A. P.; Möller, A.; Debbichi, L.; Krüger, P. M.; Iliev, N.; Gospodinov, M. M. Second-order Raman scattering in CuO. *J. Phys.: Condens. Matter.* **2013**, *25*, 105402.
(23) Romeroa, J. J.; Leret, P.; Rubio-Marcos, F.; Quesada, A.; Fernández, J. F. Evolution of the intergranular phase during sintering of $CaCu_3Ti_4O_{12}$ ceramics. *J. Eur. Ceram. Soc.* **2010**, *30*, 737.
(24) Yoo, D. K.; Yoo, S. I. Microstructures and Dielectric Properties of $CaCu_3Ti_4O_{12}$ Polycrystalline Ceramics. *Solid State Phenom.* **2007**, *124*, 143.
(25) Thongbai, P.; Jumpatam, J.; Putasaeng, B.; Yamwong, T.; Maensiri, S. The origin of giant dielectric relaxation and electrical responses of grains and grain boundaries of W-doped $CaCu_3Ti_4O_{12}$ ceramics. *J. Appl. Phys.* **2012**, *112*, 114115.
(26) Deng, G.; Xanthopoulos, N.; Muralt, P. Chemical nature of colossal dielectric constant of $CaCu_3Ti_4O_{12}$ thin film by pulsed laser deposition. *Appl. Phys. Lett.* **2008**, *92*, 172909.
(27) Ni, L.; Chen, X. M. Enhancement of Giant Dielectric Response in $CaCu_3Ti_4O_{12}$ Ceramics by Zn Substitution. *J. Am. Ceram. Soc.* **2010**, *93*, 184−189.
(28) Fang, L.; Shen, M.; Yao, D. Microstructure and dielectric properties of pulsed-laser-deposited $CaCu_3Ti_4O_{12}$ thin films on $LaNiO_3$ buffered $Pt/Ti/SiO_2/Si$ substrates. *Appl. Phys. A: Mater. Sci. Process.* **2005**, *80*, 1763−1767.
(29) Lin, S. Y.; Chen, Y. C.; Wang, C. M.; Kao, K. S.; Chan, C. Y. Effect of Rapid Thermal Annealing on Sputtered $CaCu_3Ti_4O_{12}$ Thin Films. *J. Electron. Mater.* **2009**, *38*, 453−459.
(30) Prakash, B. S.; Varma, K. B. R.; Michau, D.; Maglione, M. Deposition and dielectric properties of $CaCu_3Ti_4O_{12}$ thin films

deposited on $Pt/Ti/SiO_2/Si$ substrates using radio frequency magnetron sputtering. *Thin Solid Films* **2008**, *516*, 2874−2880.
(31) Kim, B. K.; Lee, H. S.; Lee, J. W.; Lee, S. E.; Cho, Y. S. Dielectric and Grain-Boundary Characteristics of Hot Pressed $CaCu_3Ti_4O_{12}$. *J. Am. Ceram. Soc.* **2010**, *93*, 2419−2422.
(32) Capsoni, D.; Bini, M.; Massarotti, V.; Chiodelli, G.; Mozzatic, M. C.; Azzoni, C. B. Role of doping and CuO segregation in improving the giant permittivity of $CaCu_3Ti_4O_{12}$. *J. Solid State Chem.* **2004**, *177*, 4494−4500.